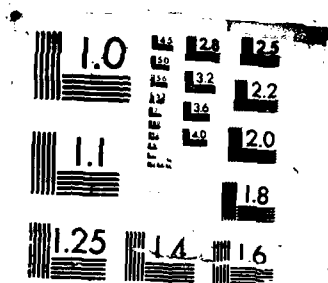AD-A133 486   PASSIVE RANGING WITH THE SNAP MODEL: A PERFORMANCE   1/1
STUDY U SACLANT ASW RESEARCH CENTRE LA SPEZIA (ITALY)
E J SULLIVAN ET AL JUL 87 SACLANTCEN-CP-118

UNCLASSIFIED   F G 17/1   NL

END
DATE
FILMED
?-87

MICROCOPY RESOLUTION TEST CHART

AD-A183 486

DTIC FILE COPY

SACLANT ASW
RESEARCH CENTRE
REPORT

DTIC
ELECTE
AUG 1 4 1987
D

Passive ranging with
the SNAP model:
A performance study

E.J. Sullivan
and K. Rameau

July 1987

7 08

Page count for SR-118
(excluding covers)

Pages	Total
i–iv	4
1–11	11
@1–@10	10
	25

SACLANT ASW Research Centre
Viale San Bartolomeo 400
19026 San Bartolomeo (SP), Italy

tel: 0187 540 111
telex: 271148 SACENT I

NORTH ATLANTIC TREATY ORGANIZATION

Passive ranging with
the SNAP model:
A performance study

E.J. Sullivan and K. Rameau

Raleu R Goodman

Ralph R. Goodman
Director

Passive ranging with the SNAP model:
A performance study

E.J. Sullivan and K. Rameau

Abstract: A passive ranging technique which uses SNAP, the SACLANT
Centre's normal-mode model, is studied. An examination is made of the
sensitivity of the technique to errors in the assumed sound velocity profile
and tilting of a 16λ vertical receiving array. Also, the effect of both white
and coloured noise is investigated. Results indicate that for the scenario
considered (summer profile in the Mediterranean with a water depth of
130 m and source ranges of 10 and 25 km), the method can be quite robust
to sound velocity profile errors or the order of several m/s and array tilts
on the order of 1.5°. Solutions were obtained with input signal-to-noise
ratios as low as −13 dB.

Keywords: array tilt o bottom properties o coloured noise o depth
o gaussian noise o inverse problem o maximum likelihood o passive
ranging o propagation o sensitivity o signal-to-noise ratio o SNAP o
sound velocity profile o white noise

Contents

1. Introduction

Given a sufficiently accurate oceanic propagation model and a sufficiently accurate set of parameters for this model, one can solve either of the following two problems: (1) given enough information concerning one or more acoustic sources, find the resulting acoustic field anywhere in the ocean; (2) given a sufficient sample of the acoustic field in the ocean, find the position of the source(s). Problem (1) is commonly referred to as the forward problem whereas problem (2) has become known as the inverse problem. In this report we are concerned with the inverse problem and more specifically the effects of errors in the input parameters on such a problem.

2. Theory

Our particular inverse problem is defined as follows. Given the measurements from a set of equally-spaced hydrophones on a vertical array, find the range to the narrow-band acoustic point source. The approach is based on the fact that the normal-mode model of propagation permits a set of linear equations to be written that can be inverted. For fixed frequency, range and water density, the normal-mode model expresses the far-field acoustic pressure at range r and depth z as

$$P(r, z) = \sum_{n=1}^{N} \frac{\phi_n(z)\phi_n(z_0)}{\sqrt{k_n}} e^{-\alpha_n r + i k_n r}. \tag{1}$$

Here, $\phi_n(z)$ is the nth modal function at depth z, z_0 is the depth of the source, α_n is the loss function for the nth mode, k_n is the horizontal wave number for the nth mode, and N is the total number of modes

A more comprehensive discussion of Eq. (1) can be found in [1, 2]. For our purposes it is sufficient to say that Eq. (1) represents a range-independent model and therefore the modal function loss factor and the horizontal wave number all can be computed with knowledge of the sound velocity profile (SVP), water depth and bottom properties but without knowledge of the range. Furthermore, since the modal functions are real, the range information is contained in the phase only, and therefore the source depth need not be known.

Defining

$$M_{m,n} = \phi_n(z_m)/\sqrt{k_m}, \tag{2a}$$

$$A_n = \phi_n(z_0)e^{\alpha_n r}, \tag{2b}$$

$$\chi_n = A_n e^{ik_n r}, \tag{2c}$$

Eq. (1) can be written as

$$P_m = M_{m,n} \chi_n. \tag{3}$$

Inversion of Eq. (3) yields the N functions χ_n which, in principle, can be solved for the range. With the addition of noise, Eq. (3) becomes

$$P_m = M_{m,n} \chi_n + \varepsilon_m, \qquad 1 \le n \le N,$$
$$1 \le m \le M, \tag{4}$$

where M is the number of hydrophones and, as defined previously, N is the number of modes supported by the acoustic channel. For the case of gaussian noise, the maximum-likelihood estimate of χ_n for the case of $M > N$, is given by [3]:

$$\hat{\chi} = (M^\dagger R^{-1} M)^{-1} M^\dagger R^{-1} P, \tag{5}$$

where the noise covariance matrix R is defined by $R = E\{\varepsilon\varepsilon^\dagger\}$. E denotes expected value and $\dagger$ signifies complex conjugate transpose.

The present study assumes white noise whereby Eq. (5) reduces to

$$\hat{\chi} = VP \tag{6}$$

with

$$V = (M^\dagger M)^{-1} M^\dagger. \tag{7}$$

This can be seen by substituting $R = \sigma^2 I$ in Eq. (5). Here I is the identity matrix.

Equation (5) provides the maximum-likelihood solution for $\hat{\chi}$, whereas we are concerned with the estimation of r. The algebraic solution for r from $\hat{\chi}$ however, is a maximum-likelihood estimator of r if $\hat{\chi}$ is the maximum-likelihood estimate of χ. This is guaranteed by the invariance of maximum-likelihood estimates [4].

A convenient form for the solution and, in particular, for our sensitivity study can be found by defining a 'solution matrix' as

$$S = \langle \chi \chi^\dagger \rangle, \tag{8}$$

where the brackets indicate time average. Writing the pressure vector explicitly in terms of the noise-free signal, we have

$$P = P_0 + \varepsilon. \tag{9}$$

Thus, from Eqs. (6), (8) and (9) we find

$$S = V(P_0 P_0^\dagger)V^\dagger + VRV^\dagger. \tag{10}$$

- 2

Equation (10) is derived based on the assumption that the signal and noise are uncorrelated. Since, as pointed out earlier, the modal functions are real, the range can be computed from the phase information alone. Thus, from Eq. (2c), one obtains

$$\arg(S_{ij}) = (k_i - k_j)r - \pi N, \tag{11}$$

where S_{ij} is the ijth element of the solution matrix S. The term πN is necessary since $\arg(S_{ij})$ only provides the principle value of the phase and the sign of ϕ_n of Eq. (2a) is not known. Solving for r yields

$$r_{ij} = \frac{\arg(S_{ij})}{(k_i - k_j)} + N\frac{\pi}{(k_i - k_j)}. \tag{12}$$

Defining

$$r_{ij}^0 = \frac{\arg(S_{ij})}{(k_i - k_j)}, \qquad \Delta r_{ij} = \frac{\pi}{(k_i - k_j)},$$

Eq. (12) becomes

$$r_{ij} = r_{ij}^0 + N\Delta r_{ij}. \tag{13}$$

Since Eq. (13) is clearly multiple-valued, we must as a minimum introduce a third mode. Upon introduction of, say, mode k, we would have three solutions: r_{ij}, r_{ik} and r_{jk}. Generally, for q modes, the number of solutions is given by the binomial coefficient $q!/2!(q - 2)!$, i.e. the number of ways q things can be taken 2 at a time. If the solutions are computed out to some maximum range and the number of solutions are counted up in range bins, a plot can be constructed indicating the number of solutions per range bin. This is illustrated in Fig. 1. Here we see the number of solutions plotted for the cases of 4, 6, 8 and 10 modes, all of which indicate 25 km as the solution. This could be thought of as a pseudo probability density function. The bin size here and in all following plots is 100 m.

3. Sensitivity study

Generally speaking, a sensitivity study of the type of problem considered here could ask two separate questions: (1) How sensitive is the algorithm to errors in the measured field quantities? (2) How sensitive is the algorithm to errors in the channel parameters (model parameters)? This issue is discussed in detail in the appendix. Here we are interested in question number (2). In particular, we will look at the sensitivity to errors in the SVP and the deviation of the array from the vertical (array tilt). Also, we will investigate the performance of the algorithm in the presence of noise.

The sensitivity to errors in the SVP and array angle were calculated based on the scheme shown in Fig. 2, which uses the SVP as an example. A synthetic data set is computed based on the 'true' SVP, i.e. $(SVP)_0$. The signal that would be received on the array, P_0, is then computed. This synthetic data set is based on the modal functions designated as $\{\phi_n\}_0$. This then is a standard forward problem. Next a different SVP, designated (SVP), is assumed. This differs from $(SVP)_0$ in some prescribed way and represents the error introduced by our ignorance of the true value. A new set of modal functions is then computed. From these modal functions, designated $\{\phi_n\}$, the matrix V (see Eq. (7)) is computed. The solution matrix and the range are then computed. This range, designated as r' in Fig. 2, is then compared with V, the range used in the computation of the synthetic data vector P_0.

For the calculations with noise, the prescribed noise matrix is used in Eq. (10). More specifically the signal matrix $PP^\dagger$ was defined where

$$PP^\dagger \quad \binom{S}{N} \frac{P_0 P_0^\dagger}{\text{Tr}(P_0 P_0^\dagger)} + \frac{R}{T_r(R)}, \qquad (14)$$

where Tr designates trace.

The scenario for the study consists of an acoustic channel with a constant (in range) depth of 130 m. A point source of 190 Hz is placed at a depth of 50 m and a vertical array of 32 equally spaced hydrophones samples the acoustic field at ranges of 10 and 25 km. This configuration, along with the bottom parameters, is summarized in Fig. 3. This corresponds to the area of the Mediterranean north of the island of Elba. The bottom parameters were taken from [5]. The sound velocity profiles were based on measurements taken in the North Elba area during the summer of 1986.

3.1. SENSITIVITY TO SVP

As mentioned previously, the sound velocity data were based on measurements made during the summer in the area of interest. Figure 4 depicts the spread of

these measurements (slightly smoothed for convenience) with the mean, which was chosen as $(SVP)_0$. The parameter α is a measure of the deviation of the SVP (represented by the dotted curve) from $(SVP)_0$. In Fig. 4 $\alpha = 0.2$ which means that the dotted curve is displaced 20% of the distance between $(SVP)_0$ and the maximum, i.e. the rightmost curve. Thus, the dotted curve in Fig. 4 represents an SVP error which constitutes a displacement from $(SVP)_0$. This will be referred to as an error of the first type. A second type of error was investigated. This is depicted in Fig. 5. Here the sign of the deviation is alternated, thus producing a short-scale type error. This will be referred to as an error of the second type. The results are shown in Figs. 6-12.

Figures 6 and 7 show the results for a range of 25 km for errors of the first type for $\alpha = 0.1$ and 0.2. These values of α correspond roughly to sound speed deviations on the order of 0.5 and 1.0 m/s, respectively. Two things can be seen from these figures. First, the algorithm is quite sensitive to SVP errors of this type and second, the error impacts the higher order modes more severely. Turning to the second type of SVP error, Figs. 8 and 9, which also depict the 25 km range case, indicate that the results are much less sensitive to errors of this type.

Here values of α as high as 0.3 (2-3 m/s) can be tolerated where for errors of the first type, values of α greater than 0.1 cannot be tolerated.

What is more interesting is that errors of the second type appear to affect the lower-order modes more strongly than the higher-order modes—quite the opposite of the case for the errors of the first type.

Figures 10 and 11 depict the results for a range of 10 km for errors of the first type for $\alpha = 0.1$ and 0.5. Here we come to the not too surprising conclusion that the errors compound with increasing range. Also, it can be seen that the result is biased, i.e. the range tends to be underestimated.

Figure 12 depicts the 10 km case for an error of the second type with $\alpha = 0.5$. Again, we see that the algorithm is less sensitive to this type of error. As before, we find the conclusion that shorter ranges can support greater SVP errors. Finally we note that, as with the 25 km results, errors of the first type tend mainly to impact the higher-order modes whereas errors of the second type tend to impact the lower-order modes.

3.2. SENSITIVITY TO ARRAY TILT

Turning to the sensitivity of the algorithm to the tilting of the array we refer first to Figs. 13 and 14. Here the cases for ranges of 10 km and 25 km is depicted respectively. As can be seen, for a tilt of 0.5°, the solution is seriously degraded. Beyond a tilt of 1.0°, the solution is lost.

The sensitivity to array tilt can be easily understood by the following argument. We begin by writing Eq. (6) out in explicit matrix form:

$$
\begin{bmatrix} \lambda_1 \\ \lambda_2 \\ \vdots \\ \lambda_{10} \end{bmatrix} = \begin{bmatrix} V_{1,1} & V_{1,2} & \cdots & V_{1,32} \\ V_{2,1} & V_{2,2} & \cdots & V'_{2,32} \\ \vdots & \vdots & \vdots & \vdots \\ V_{10,1} & V_{10,2} & \cdots & V_{10,32} \end{bmatrix} \cdot \begin{bmatrix} P_1 \\ P_2 \\ \vdots \\ P_{32} \end{bmatrix}.
\tag{15}
$$

Here, we see that each row of the matrix V functions as a beamformer that functions as a spatial modal filter.

In the normal-mode model each mode propagates as a plane wave (albeit with a depth-dependent amplitude). Thus, if we apply, say, mode 1 to row 1 of V this should extract mode 1 and reject all the others. The plane wave beam pattern that obtains when mode 1 is applied to row 1 is plotted in Fig. 15. Here we see the expected result of maximum response at $0°$(horizontal). When mode 2 is applied to row 1, however, the beam pattern shown in Fig. 16 results. We see the expected notch indicating the rejection of the mode. The narrowness of the notch indicates that a slight tilting of the array will allow energy from the other modes to spill in, thus explaining the sensitivity of the algorithm to the angle of the array.

4. Noise study

The effect of noise on the algorithm was investigated for the case of gaussian noise, both white and coloured. The results for the white noise case are shown in Figs. 17 and 18 which correspond to the cases for a signal-to-noise ratio of -13 dB. As can be seen from Eq. (14), the signal-to-noise ratio is that as seen by a single hydrophone, i.e. it is the input signal-to-noise ratio. The algorithm broke down at $S/N = -15$ dB.

The results for the case of coloured noise indicated no significant difference and hence are not included here.

Although these results indicate quite good performance in the presence of noise, they appear consistent with the fact that the array gain is of the order of 15 dB.

5. Discussion

There are two interesting conclusions that can be drawn from the SVP study. The first is that the results are strongly influenced by the spatial scale of the SVP error. The second conclusion is that which modes are affected by the error is strongly influenced by the spatial scale of the SVP error. Thus, based on these results, one sees that it is the large-scale errors that are most inportant. This result is quite important since it implies that making a search of possible SVPs in the solution is feasible. Since only the large-scale properties of the profile are important, the class of profiles that would have to be scanned is reasonably small, since fine structure is of lesser importance. In this study the errors of the second type involved scales on the order of one wavelength.

This insensitivity to SVP fine structure suggests a possible extention of a technique such as this to the active sonar case. With a single active sonar ping, one can determine the range to a target. Given this range and some knowledge of the channel (i.e. depth, bottom conditions and incomplete SVP information) one could, via such a search method, conceivably improve knowledge of the SVP. This suggests a type of in-situ environmental parameter update scheme.

The possibility of solutions based on parameter searches as discussed above also presents itself in the case of array tilt. Since the results indicate stability to array tilts on the order of 1°, a search of array angles would present little difficulty. The question of array curvature, however, is more problematical. Preliminary studies indicate that the algorithm is quite sensitive to modest curvatures. Dealing with this problem by such search techniques certainly would be more computationally intensive.

As mentioned in Sect. 4 the performance in the presence of noise is quite good. This is quite surprising in view of the sensitivity of the algorithm to phase errors in general (SVP errors and array tilt). However, as pointed out previously, it is not inconsistent if one considers that the array gain may be playing a role here.

Appendix A
Measurements, models and sensitivity studies

In the case of passive localization, the problem would proceed as follows. A propagation model is selected (a normal-mode model might suffice for the shallow-water low-frequency case). Parameters required by the model are then obtained by measurement or from archival data. Measurements of the acoustic field are then taken and the position of the acoustic source is estimated via some algorithm. This is depicted in Fig. A1.
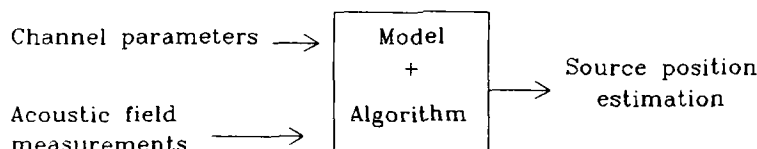
Channel parameters $\longrightarrow$ Model + Algorithm $\longrightarrow$ Source position estimation

Acoustic field measurements $\longrightarrow$

Fig. A1: Schematic diagram of passive source localization procedure.

There are now three questions that must be asked: (1) How faithful is the model? (2) How well must the channel parameters be known? (3) How well must the field quantities be known? Question (2), furthermore, has two parts: How accurate must the measurement be and how much time instability (fluctuation) can be tolerated?

Let $\dot{Z}$ be an estimated position descriptor (e.g. range). Then

$$\dot{Z} = Z_0 + \Delta Z_M + \Delta Z_P + \Delta Z_I, \tag{A1}$$

where Z_0 is the true value, ΔZ_M is the error due to field measurement errors, ΔZ_P is the error in the model parameters, and ΔZ_I is the error due to model infidelity.

The accuracy of the estimation of Z_0 depends upon all three error terms whereas the precision is determined only by ΔZ_M and ΔZ_P. Thus a sensitivity study carried out with a given model can only determine the sensitivity of $\dot{Z}$ to errors in the parameters and field quantities. That is, the sensitivity study can only answer questions concerning precision (questions (2) and (3)) and not accuracy. The accuracy question must be settled as the second step in the process. That is,

given a model a sensitivity study is carried out. If the results indicate that the problem is tractable (i.e. ΔZ_M and ΔZ_P can be rendered small enough), a series of measurements must then be performed to determine whether ΔZ_I is small enough to allow a useful (sufficiently accurate) estimation of the range.

A.1. SENSITIVITY

The sensitivity problem can be stated as follows. Given small changes in the measured inputs to the model, what is the corresponding change produced in the desired quantity? Thus

$$\Delta Z_M = \sum_i \alpha_i dx_i, \tag{A2}$$

$$\Delta Z_P = \sum_i \beta_i dy_i, \tag{A3}$$

where

$$\alpha_i = \left\{ \frac{\partial Z}{\partial x_i} \right\}, \qquad \beta_i = \left\{ \frac{\partial Z}{\partial y_i} \right\},$$

and $\{x_i\}$ and $\{y_i\}$ are the field quantities and the model parameters, respectively. The sensitivity problem then, is the determination of the $\{\alpha_i\}$ and $\{\beta_i\}$.

As stated so far the issue seems to be quite straightforward. Via model studies, one determines the sensitivity parameters $\{\alpha_i\}$ and $\{\beta_i\}$ and compares them. If the $\{\alpha_i\}$ in conjunction with the existing margin of uncertainty in the field measurements are the major source of error then better measurements are called for. If, on the other hand, the $\{\beta_i\}$ indicate that the sensitivity to the model parameters is the major source of error, the problem becomes more complicated, since the issue of fluctuations arises. It may simply not be sufficient to improve the accuracy of the parameter measurements since the parameters themselves may be fluctuating in time. (The question of spatial fluctuations we consider to be included in the issue of model fidelity.) If this is the case, and the errors due to these fluctuations are intolerable, the only possible course would be to modify the model to include them, given that the physics is known and tractable. It should be noted here that such a course would only guarantee that the model is sufficiently sensitive and not necessarily faithful. That is, the model may be precise enough but still not accurate enough. Clearly though, this would constitute a necessary condition for a faithful model. Since the new model will undoubtedly require a new sensitivity study, it most likely will follow that more stringent measurement requirements will arise for the field measurements. Of course, this would have been obvious from the fact that the fluctuations in the parameters would cause observable fluctuations in the measured field.

At first glance, the approach discussed above might seem unnecessarily cumbersome. That is, why not simply do the sensitivity analysis in the 'forward sense'?

- 9 -

This could be done by varying the target location in a systematic manner and observing the variations in the computed field. The problem with this is that it is not clear how such field variations are related to the efficacy of the algorithm. This problem is avoided in the approach under discussion here since the complexities of the model and the algorithm are all contained in the $\{\alpha_i\}$ and $\{\beta_i\}$. It simply does not follow that if a given error, say ΔZ, in the source location produces a given change in phase or amplitude of the field such phase or amplitude fluctuations in the measured field limit the determination of the source location to ΔZ.

A trivial example of this fact is provided by the case of a random variation in the amplitude of a narrow-band source, where the fluctuations introduced are assumed to be made up of frequencies much lower than that of the source. Clearly in this case, the wavenumber properties of the field, which are the properties pertinent to the spatial processing aspects of our problem, are essentially unchanged.

References

[1] SULLIVAN, E.J. Passive localization with propagation models. SACLANTCEN SR-117, La Spezia, Italy, SACLANT ASW Research Centre, 1987.

[2] JENSEN, F.B. and FERLA, M.C. SNAP: The SACLANTCEN Normal-Mode Acoustic Propagation model. SACLANTCEN SM-121, La Spezia, Italy, SACLANT ASW Research Centre, 1979. [AD A 067 256]

[3] WHALEN, A.D. Detection of Signals in Noise. New York, Academic Press, 1971.

[4] COX, D.R. and HINKLEY, D.V. Theoretical Statistics. London, Chapman and Hall, 1982: p. 287.

[5] AKAL, T. et al. Acoustic transmission loss data for some selected shallow-water areas. SACLANTCEN SR-33, La Spezia, Italy, SACLANT ASW Research Centre, 1979. [AD C 950 788]
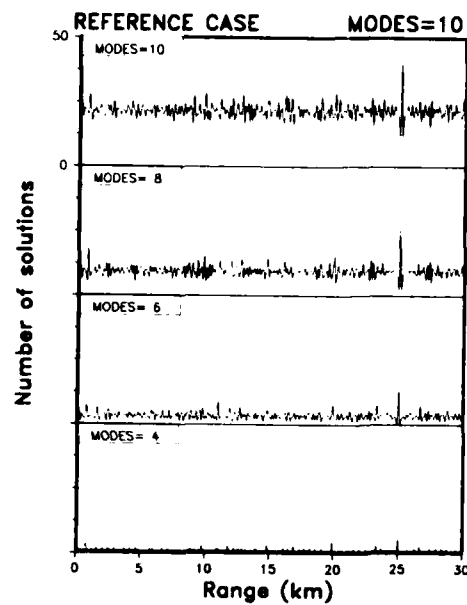
REFERENCE CASE   MODES=10

Fig. 1: Plot of solutions for the case of 25 km range. The number of solutions per range bin is plotted as a function of range. The bin size is 100 m.
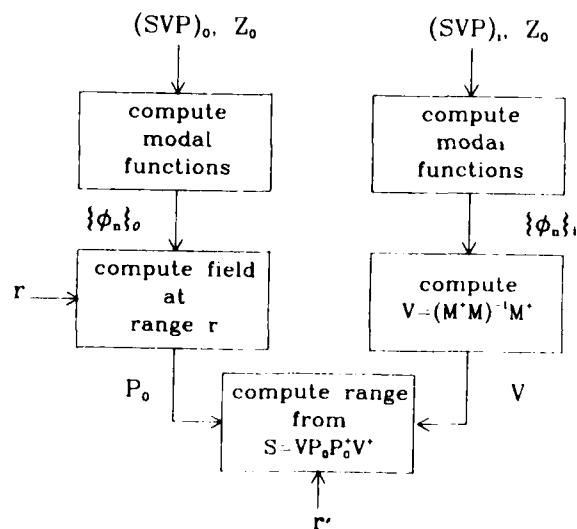

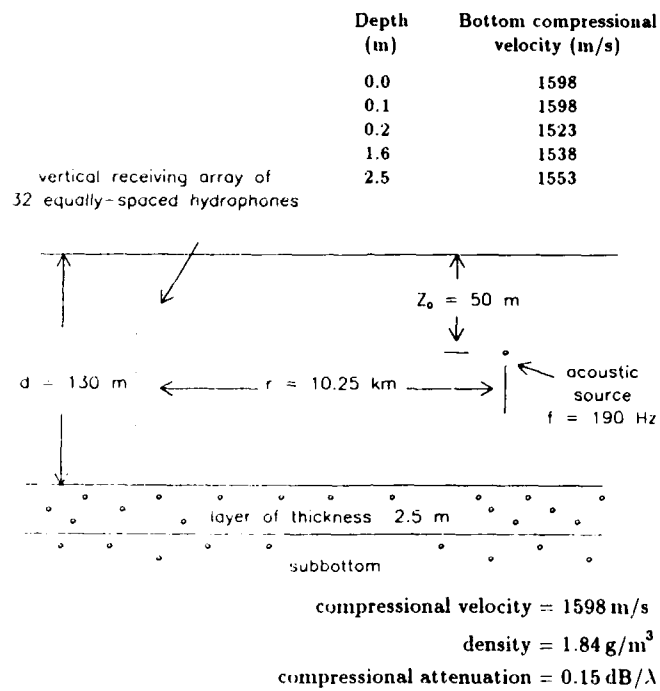*Fig. 2:* Schematic diagram of sensitivity study computation.

Depth (m)	Bottom compressional velocity (m/s)
0.0	1598
0.1	1598
0.2	1523
1.6	1538
2.5	1553

vertical receiving array of
32 equally-spaced hydrophones

$Z_o = 50$ m

d = 130 m $\longleftarrow$ r = 10.25 km $\longrightarrow$ acoustic source
f = 190 Hz

layer of thickness 2.5 m

subbottom

compressional velocity = 1598 m/s

density = $1.84\,\text{g/m}^3$

compressional attenuation = $0.15\,\text{dB}/\lambda$

Fig. 3: Source-receiver configuration and acoustic channel parameters.

Sound Speed (m)

Depth (m)	Sound speed (m/s)
0.0	1539.6
5.0	1539.4
10.0	1536.5
15.0	1531.3
20.0	1525.8
25.0	1521.7
30.0	1517.5
35.0	1514.5
40.0	1512.1
50.0	1510.0
60.0	1508.8
80.0	1507.7
100.0	1507.5
120.0	1507.7
130.0	1507.7
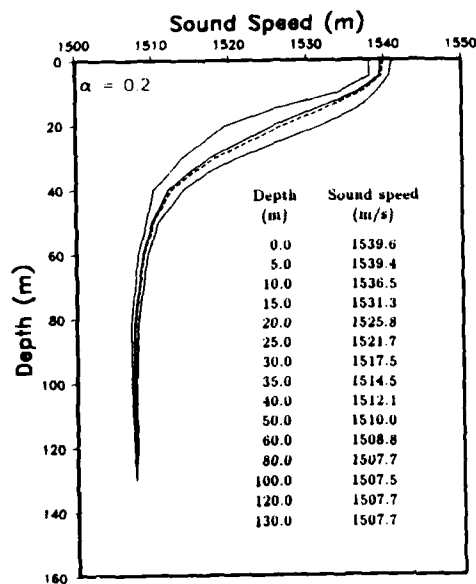
Fig. 4: Experimental SVP for the region north of Elba. The central profile is the average of a two-week series of measurements. The outer curves depict the spread of the measurements and the dashed curve represents a displacement of the average SVP. In the text this is referred to as an error of the first type. Here, the displacement is 20% of the distance between the average and the maximum, and is denoted by a value of 0.2 for the parameter α. The numerical values are those of the mean.

Sound Speed (m)
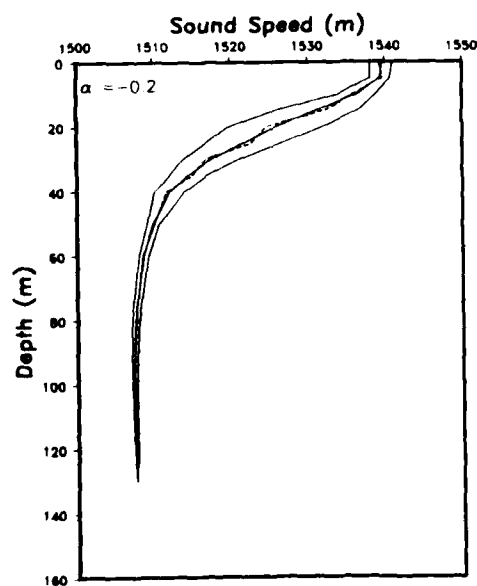
Fig. 5: SVP error of the second type. This curv. is identical to that of Fig. 4 except that the displacements alternate in sign.
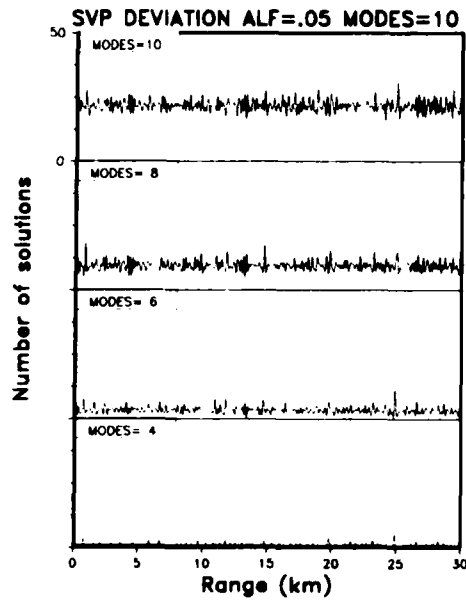
93

Fig. 6: Results for an SVP error of the first type. Here α is 0.05, which constitutes a deviation of 5% of the total spread, and the true range is 25 km.
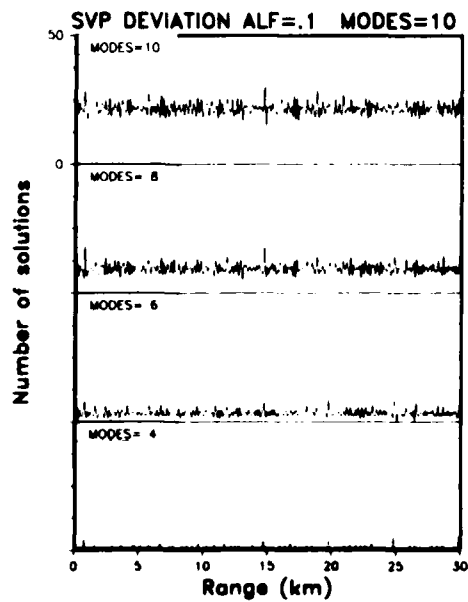

Fig 7 Results for an SVP error of the first type: α 0.1 and the true range is 25 km
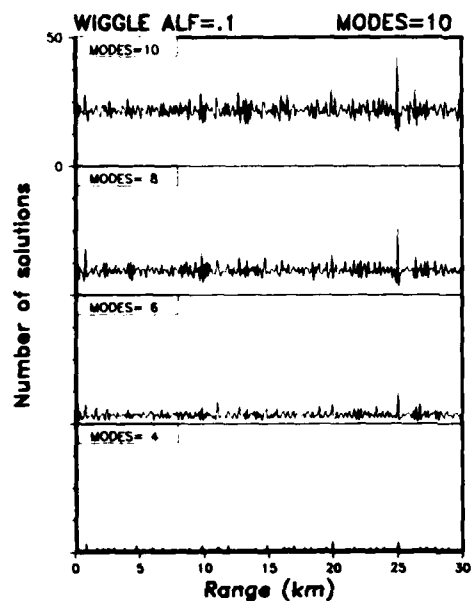
Fig. 8: Results for an SVP error of the second type: $\alpha = 0.1$ and the true range is 25 km.

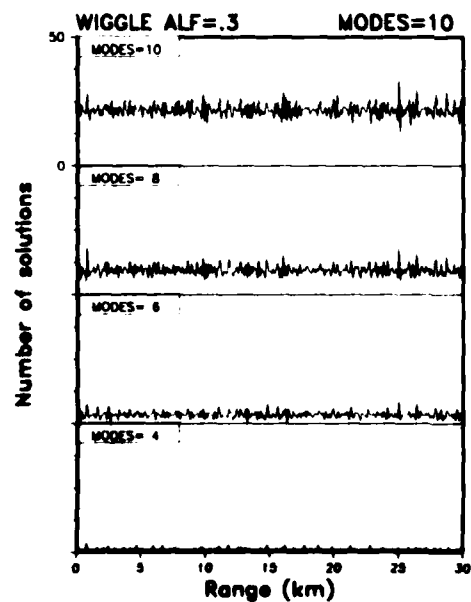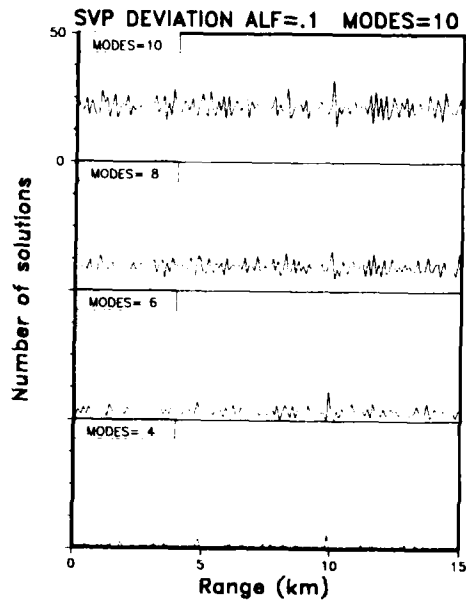Fig. 9: Results for an SVP error of the second type: $\alpha = 0.3$ and the true range is 25 km.

SVP DEVIATION ALF=.1 MODES=10

Fig. 10: Results for an SVP error of the first type: $\alpha = 0.1$ and the true range is 10 km.
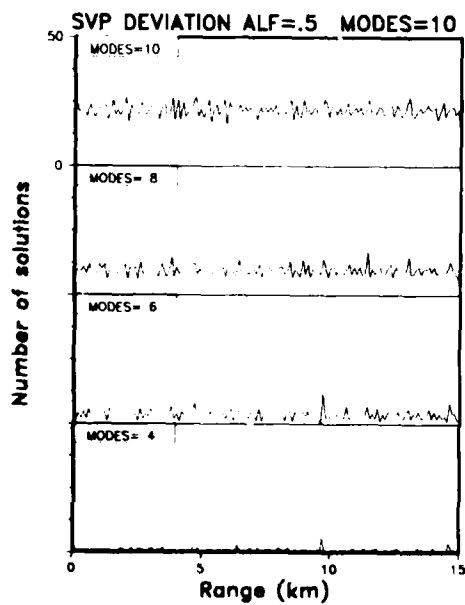
SVP DEVIATION ALF=.5 MODES=10

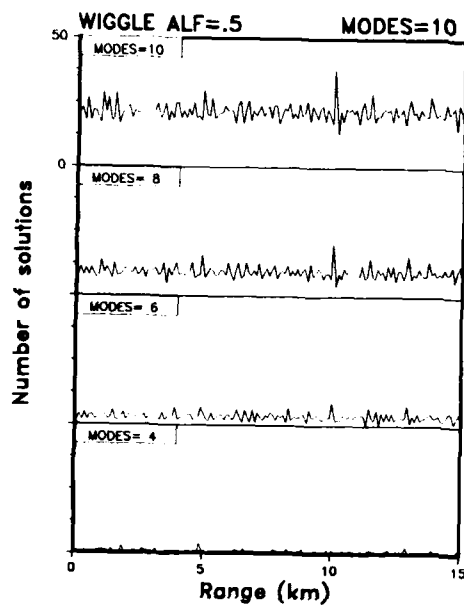Fig. 11: Results for an SVP error of the first type: $\alpha = 0.5$ and the true range is 10 km.

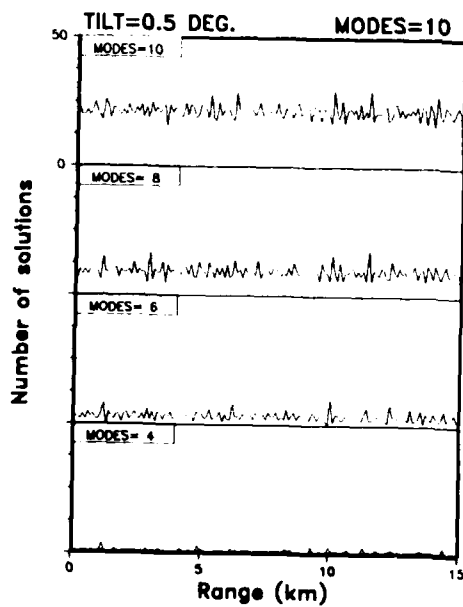Fig. 12: Results for an SVP error of the second type: $\alpha = 0.5$ and the true range is 10 km.

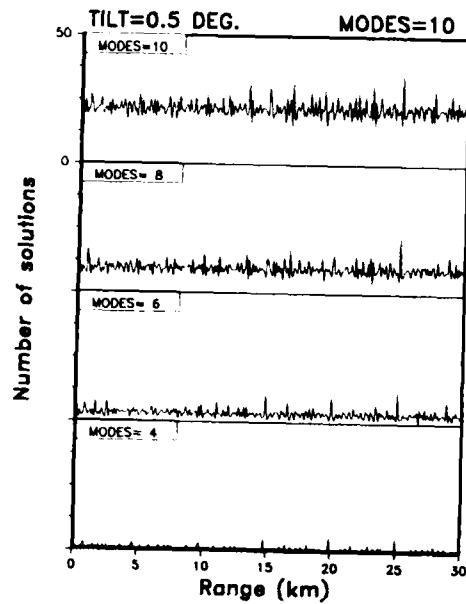Fig. 13: Results for an array tilt of 0.5°: the true range is 10 km.

TILT=0.5 DEG.   MODES=10

MODES=10

MODES= 8

MODES= 6

MODES= 4

Number of solutions

Range (km)

Fig. 14: Results for an array tilt of 0.5°: the true range is 25 km.

filter 1; mode1; k1

Amplitude (dB)

Degrees

Fig. 15: Angular response of the vertical array to mode no. 1: the beamformer weights are the modal filter coefficients for mode no. 1.

filter 1; mode2; k2

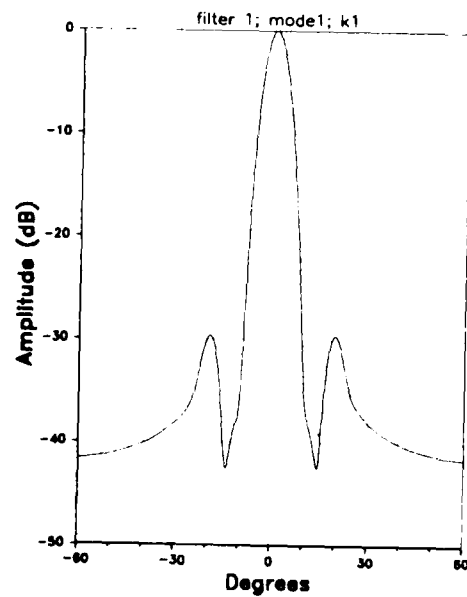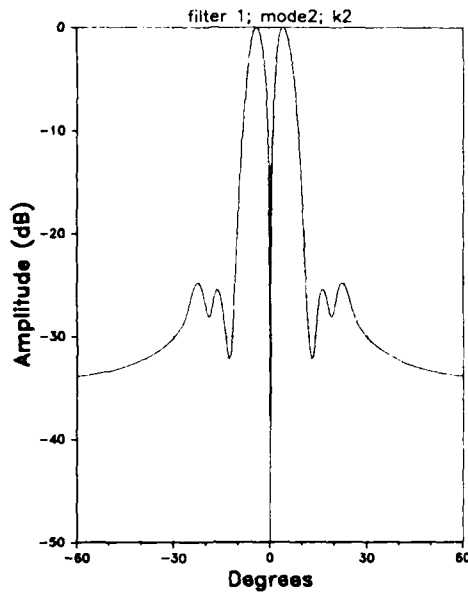*Fig. 16:* Angular response of the vertical array to mode no. 2: the beamformer weights are the modal filter coefficients for mode no. 1.

SNR=-13 DB WHITE   MODES=10

MODES=10
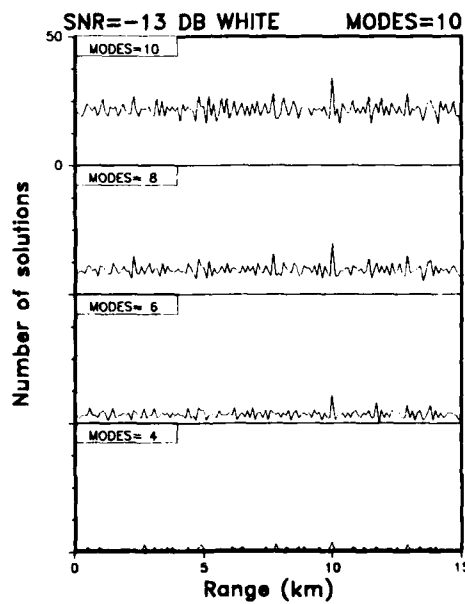
MODES= 8

MODES= 6

MODES= 4

Fig. 17: Results for the case of white gaussian noise: the signal-to-noise ratio is -13 dB and the true range is 10 km.
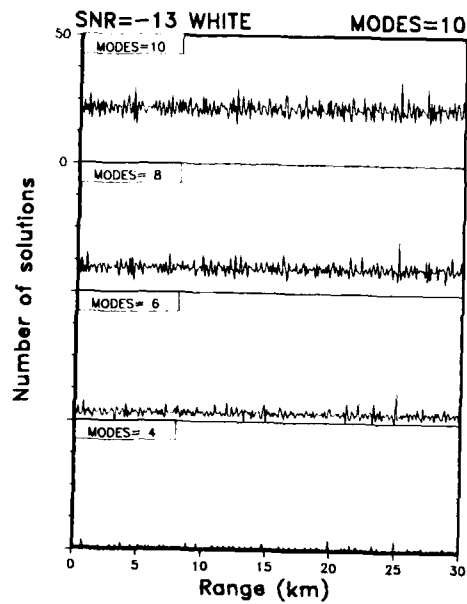
Fig. 18: Results for the case of white gaussian noise: the signal-to-noise ratio is −13 dB and the true range is 25 km.

Initial Distribution for SR-118

Ministries of Defence

JSPHQ Belgium	2
DND Canada	10
CHOD Denmark	8
MOD France	8
MOD Germany	15
MOD Greece	11
MOD Italy	10
MOD Netherlands	12
CHOD Norway	10
MOD Portugal	2
MOD Spain	2
MOD Turkey	5
MOD UK	20
SECDEF US	68

NATO Authorities

Defence Planning Committee	3
NAMILCOM	2
SACLANT	10
SACLANTREPEUR	1
CINCWESTLANT/ COMOCEANLANT	1
COMSTRIKFLTANT	1
COMIBERLANT	1
CINCEASTLANT	1
COMSUBACLANT	1
COMMAIREASTLANT	1
SACEUR	2
CINCNORTH	1
CINCSOUTH	1
COMNAVSOUTH	1
COMSTRIKFORSOUTH	1
COMEDCENT	1
COMMARAIRMED	1
CINCHAN	3

SCNR for SACLANTCEN

SCNR Belgium	1
SCNR Canada	1
SCNR Denmark	1
SCNR Germany	1
SCNR Greece	1
SCNR Italy	1
SCNR Netherlands	1
SCNR Norway	1
SCNR Portugal	1
SCNR Turkey	1
SCNR UK	1
SCNR US	2
SECGEN Rep. SCNR	1
NAMILCOM Rep. SCNR	1

National Liaison Officers

NLO Canada	1
NLO Denmark	1
NLO Germany	1
NLO Italy	1
NLO UK	1
NLO US	1

NLR to SACLANT

NLR Belgium	1
NLR Canada	1
NLR Denmark	1
NLR Germany	1
NLR Greece	1
NLR Italy	1
NLR Netherlands	1
NLR Norway	1
NLR Portugal	1
NLR Turkey	1
NLR UK	1

Total external distribution	248
SACLANTCEN Library	10
Stock	22
Total number of copies	280

END

DATE
FILMED

9-87